Probing the Structure of Immobilized Metal Sites in Porous Organic Hosts by X-ray Absorption Spectroscopy

Karen M. Padden,[†] John F. Krebs,[†] Katherine T. Trafford,[‡] Glenn P. A. Yap,[§] Arnold H. Rheingold,[§] A. S. Borovik,*[,†] and Robert C. Scarrow*[,‡]

Department of Chemistry, University of Kansas, Lawrence, Kansas 66045, Department of Chemistry, Haverford College, Haverford, Pennsylvania 19041, and Department of Chemistry, University of Delaware, Newark, Delaware 19716

Received May 21, 2001. Revised Manuscript Received August 3, 2001

Template copolymerization methods have been used to make materials for a wide variety of applications where site-specific analyte binding is desired. The structure of the binding site is often crucial to the efficient function of the material. We have immobilized cobalt-containing template complexes in porous organic hosts, allowing the use of spectroscopy to conveniently probe the site structure. Reported herein are results from X-ray diffraction and X-ray absorption spectroscopy (XAS) studies for a series of monomers {[Co^{III}**1**$(dmap)_2$]-[PF_6] and [Co^{III}**2**(1-MeIm)][PF_6], where **1** is the ligand bis[2-hydroxy-4-(4-vinylbenzylmethoxy)benzaldehyde]ethylenediimine and **2** is bis[2-hydroxy-4-(4-vinylbenzylmethoxy)-benzyliminopropyl]methyl amine} and related copolymers. Copolymerization of the 6-coordinate complex [Co^{III}**1**$(dmap)_2$][PF_6] with an organic cross-linker forms immobilized 6-coordinate cobalt sites in P-**1**[$Co^{III}(dmap)_2$]. Similar findings were obtained for the formation of immobilized cobalt sites in P-**2**[Co^{III}(1-MeIm)]. Demetalation of P-**1**[$Co^{III}(dmap)_2$] and P-**2**[Co^{III}-(1-MeIm)] affords immobilized sites that contain tetra- or pentadentate ligands, respectively. Rebinding of Co^{II} ions affords P-**1**[Co^{II}] with sites containing cobalt complexes having square planar coordination geometry, whereas P-**2**[Co^{II}] has immobilized square pyramidal cobalt complexes. XAS studies support these coordination geometry assignments and show that the rigidity of the porous host maintains site architecture even after chemical modification.

Introduction

Template copolymerization is an effective method for immobilizing compounds in porous organic hosts.[1,2] Network copolymers made by this method utilize monomeric precursors as building blocks (i.e., templates and cross-linking agents) and have been used in a variety of applications, such as in separation science,[1,3] catalysis,[4] and sensing.[5] For these applications, the structure of the immobilized sites is essential for function. However, site structures are often difficult to determine and are usually inferred from data obtained through batch rebinding or mechanistic studies. Difficulties in determining the immobilized site structure arise because organic templates are used in the majority of materials made by template copolymerization methods.[6] The porous organic host, which is present in large excess in the copolymer, obscures analysis of immobilized site structure formed by the organic template.

We have recently reported that the structure of immobilized sites made with inorganic templates can be examined by spectroscopic methods.[7] For example, EPR spectroscopy has proven to be a powerful technique

[†] University of Kansas.
[‡] Haverford College.
[§] University of Delaware.

(1) General reviews: (a) Wulff, G. *Angew. Chem., Int. Ed. Engl.* **1995**, *34*, 1812−1832 and references therein. (b) Mosbach, K.; Ramstrom, O. *Biotechnology* **1996**, *14*, 163−170. (c) Shea, K. J. *Trends Polym. Sci.* **1994**, *A32*, 166−172. (d) *Molecular and Ionic Recognition with Imprinted Polymers*; Bartsch, R. A., Maeda, M., Eds.; ACS Symposium Series 703; American Chemical Society: Washington, DC, 1998.

(2) Examples of polymers formed with metal templates: (a) Dhal, P. K.; Arnold, F. H. *Macromolecules* **1992**, *25*, 7051−7059. (b) De, B. B.; Lohray, B. B.; Sivaram, S.; Dhal, P. K. *Macromolecules* **1994**, *27*, 1291−1296. (c) Santora, B. P.; Larsen, A. O.; Gagné, M. R. *Organometallics* **1998**, *17*, 3138−3140. (d) Chen, H.; Olmstead, M. M.; Albright, R. L.; Devenyi, J.; Fish, R. H. *Angew. Chem., Int. Ed. Engl.* **1997**, *36*, 642−645. (e) Saunders, G. D.; Foxon, S. P.; Walton, P. H.; Joyce, M. J.; Port, S. N. *Chem. Commun.* **2000**, 273−274. (f) Brunkan, N. M.; Gagné, M. R. *J. Am. Chem. Soc.* **2000**, *122*, 6217−6225.

(3) For example: (a) Fujii, Y.; Matsutani, K.; Kikuchi, K. *J. Chem. Soc., Chem. Commun.* **1985**, 415−417. (b) Arnold, F. H. In *Molecular and Ionic Recognition with Imprinted Polymers*; ACS Symposium Series 703; Bartsch, R. A., Maeda, M., Eds.; American Chemical Society, Washington, DC, 1998; pp 109−118.

(4) For example: (a) De, B. B.; Lohray, B. B.; Sivaram, S.; Dhal, P. K. *Tetrahedron Asymm.* **1995**, *6*, 2105−2108. (b) Minutolo, F.; Pini, D.; Salvadori, P. *Tetrahedron Lett.* **1996**, *37*, 3375−3378. (c) Polborn, K.; Severin, K. *Chem. Commun.* **1999**, 2481−2482.

(5) For example: (a) Zeng, X.; Bzhelyansky, A.; Bae, S. Y.; Jenkins, A. L.; Murray, G. M. In *Molecular and Ionic Recognition with Imprinted Polymers*; ACS Symposium Series 703; Bartsch, R. A., Maeda, M., Eds.; American Chemical Society, Washington, DC, 1998; pp 218−237. (b) Jenkins, A. L.; Uy, O. M.; Murray, G. M. *Anal. Chem.* **1999**, *71*, 373−378.

(6) Notable exceptions: (a) Shea, K. J.; Sasaki, D. Y *J. Am. Chem. Soc.* **1991** *113*, 4109−4120. (b) Katz, A.; Davis, M. E. *Nature* **2000**, *403*, 286−289. (c) ref 2a.

(7) (a) Krebs, J. F.; Borovik, A. S. *J. Am. Chem. Soc.* **1995**, *117*, 10593−10594. (b) Krebs, J. F.; Borovik, A. S. In *Molecular and Ionic Recognition with Imprinted Polymers*; ACS Symposium Series 703; Bartsch, R. A., Maeda, M., Eds.; American Chemical Society, Washington, DC, 1998; pp 159−170. (c) Krebs, J. F.; Borovik, A. S. *Chem. Commun.* **1998**, 553−554. (d) Sharma, A. C.; Borovik, A. S. *J. Am. Chem. Soc.* **2000**, *122*, 8946−8955. (e) Padden, K. M.; Krebs, J. F.; MacBeth, C. E.; Scarrow, R. C.; Borovik, A. S. *J. Am. Chem. Soc.* **2001**, *123*, 1072−1079. (f) Sharma, A. C.; Joshi, V.; Borovik, A. S. *J. Polym. Chem. Part A: Polym. Chem.* **2001**, *39*, 888−897.

10.1021/cm010502r CCC: $20.00
Published on Web 10/12/2001

in probing the coordination geometry around immobilized Co^{II} complexes in porous organic hosts.[7c−e] These studies suggest that the porous hosts regulate the primary coordination environment around the metal ions. We now present our findings that utilize X-ray absorption spectroscopy (XAS) to further probe the structures of immobilized Co^{III} and Co^{II} complexes. Two types of templates were utilized to fabricate the polymers: [Co^{III}**1**(dmap)$_2$][PF_6] and [Co^{III}**2**(1-MeIm)][PF_6], where **1** is the ligand bis[2-hydroxy-4-(4-vinylbenzylmethoxy)benzaldehyde]ethylenediimine and **2** is bis[2-hydroxy-4-(4-vinylbenzyl-methoxy)benzyliminopropyl]-methylamine. The copolymers, P-**1**[Co^{III}(dmap)$_2$] and P-**2**[Co^{III}(1-MeIm)], are the direct result of the polymerization of the aforementioned templates, whereas P-**1**[Co^{II}] and P-**2**[Co^{II}] are formed after chemical modification of the immobilized template and subsequent rebinding of Co^{II} ions. These Co^{II} materials have been shown to be effective in reversibly binding gaseous NO and O_2.[7c−e]

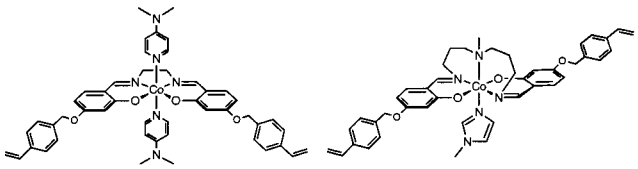

Crystallographic data for the monomeric species [Co^{III}**1**(dmap)$_2$][PF_6] and [Co^{III}**2**(1-MeIm)][PF_6] are used to evaluate the data obtained from XAS studies for the Co^{III} monomers and polymeric samples. Results from these studies demonstrate that inert metal templates retain their structural properties after copolymerization into porous organic hosts. Furthermore, the XAS data for P-**1**[Co^{II}] and P-**2**[Co^{II}] show that the structural properties of the metal ion binding sites are relatively unchanged after chemical modification, which allows for the formation of immobilized square planar and square pyramidal Co^{II} complexes, respectively, in these polymers.

Experimental Section

Solvents and reagents were used as received from either Fisher or Aldrich unless otherwise noted. Solvents used under an inert atmosphere for synthesis or sample preparation were dried following standard procedures.[8] Ethylenediamine and 3,3′-diamino-*N*-methyldipropylamine were distilled under nitrogen immediately before use. 1-Methylimidazole (1-MeIm) was distilled under nitrogen and degassed by three freeze−pump−thaw cycles. $Co(OAc)_2 \cdot 4H_2O$ was dehydrated by heating to 120 °C under vacuum for 48 h.

Synthesis of some complexes and preparation of polymerization reactions were conducted in a Vacuum Atmospheres drybox under an argon atmosphere. Standard Schlenk techniques were used during the workup of some reactions and manipulations of polymer samples outside the drybox. Elemental analyses were conducted by either Desert Analytics (Tucson, AZ), the University of Kansas Department of Medicinal Chemistry Microlab, or the analytical services laboratory of the Department of Animal Sciences at Kansas State University. The compounds 2-hydroxy-4-(4-vinylbenzylmethoxy)-benzaldehyde[9] and bis[2-hydroxy-4-(4-vinylbenzylmethoxy)benzaldehyde]ethylenediimine (H_2**1**)[7e,10] were synthesized following literature methods. The template complex [Co^{III}**1**(dmap)$_2$]-[PF_6] and polymers P-**1**[Co^{III}(dmap)$_2$] and P-**1**[Co^{II}] were synthesized as previously reported.[7e]

Bis[2-hydroxy-4-(4-vinylbenzylmethoxy)benzyliminopropyl]methylamine ($H_2$2). To a single-neck 100 mL round-bottom flask, under nitrogen atmosphere, 1.45 g (5.69 mmol) of 2-hydroxy-4-(4-vinylbenzylmethoxy)benzaldehyde was added and dissolved in methanol (25 mL) and methylene chloride (25 mL). 3,3′-Diamino-*N*-methyldipropylamine (0.414 g, 459 μL, 2.85 mmol) was then added to the flask via syringe. Approximately 5 min after addition was completed a yellow precipitate formed. The reaction was stirred for an additional 6 h, after which volatiles were removed under reduced pressure to yield a yellow solid. Yield of the yellow solid was 86% (1.507 g). ^{1}H NMR ($CDCl_3$): δ 14.06 (broad singlet, 2H, −O*H*); 8.12 (singlet, 2H, −N=C*H*(Ph)); 7.43 (d, 4H, styryl phenyl); 7.34 (d, 4H, styryl phenyl); 7.05 (d, 2H, salicyl phenyl); 6.71 (dd, 2H, 10.9 Hz, *H*(Ph)C=CH$_2$); 6.46 (d, 2H, salicyl phenyl); 6.40 (dd, 2H, salicyl phenyl); 5.75 (d, 2H, trans H(Ph)C=C*H*$_2$); 5.25 (d, 2H,cis H(Ph)C=C*H*$_2$); 5.03 (s, 4H, PhO−C*H*$_2$Ph); 3.56 (triplet, 4H, C=N−C*H*$_2$CH$_2$CH$_2$N(CH$_3$)−); 2.42 (triplet, 4H, C=N−CH$_2$CH$_2$C*H*$_2$N(CH$_3$)−); 2.21 (s, 3H, C=N−CH$_2$CH$_2$-CH$_2$N(C*H*$_3$)−); 1.83 (quintet, 4H, C=N−CH$_2$C*H*$_2$CH$_2$N(CH$_3$)−). IR (KBr): 2940 (vw), 2844 (vw), 2796 (vw), 1633 (s), 1577 (m), 1515 (m), 1454 (m), 1407 (m), 1379 (m), 1338 (w), 1302 (m, sh), 1286 (m), 1226 (m), 1185 (m), 1172 (m), 1136 (m), 1118 (m), 1046 (m), 1015 (w), 994 (w), 977 (w), 900 (w), 836 (m), 827 (m), 652 (w), 467 (w) cm^{-1}. UV−vis (CH_2Cl_2, λ_{max}/nm (ϵ, M^{-1} cm^{-1})): 258 (54 500), 266 (54 600), 299 (27 700), 388 (3530). Mp: 79−80 °C.

[Co^{III}2(1-MeIm)][PF_6]. To a 100 mL single-neck flask, under argon, was added 0.596 g (0.965 mmol) of H_2**2** (partially dissolved in 1,2-dichloroethane). A methanolic solution of $Co(OAc)_2$ (0.171 g, 0.965 mmol) was then added. After addition was completed, the mixture became yellow-brown/green in color. A methanolic suspension of ferrocenium hexafluorophosphate (0.319 g, 0.965 mmol) was added to afford a deep red-brown solution. After stirring the mixture for 12 h, 1-methylimidazole (0.0792 g, 77 μL, 0.965 mmol) was added, and after 5 min the reaction mixture turned dark green-brown. After stirring the mixture for an additional 3 h, volatiles were removed under reduced pressure to yield a dark green-brown solid. This solid was filtered and washed with diethyl ether until the diethyl ether became clear and dried under vacuum. The yield of the complex was 0.861 g (99%). Anal. Calcd for [Co^{III}**2**(1-MeIm)][PF_6]·0.5CH_2Cl_2: $C_{43}H_{47}CoF_6N_5O_4P \cdot 0.5\,CH_2Cl_2$; C, 55.33; H, 5.12; N, 7.42. Found: C, 55.20; H, 5.10; N, 7.23 (presence of the methylene chloride was corroborated by NMR spectroscopy). ^{1}H NMR ($CDCl_3$): δ 7.70 (s, 1H, −N=C*H*(Ph)); δ 7.57 (s, 1H, −N=C*H*(Ph)); 7.4 (m, 9H, styryl phenyl (8H) and imidazole (1H)); 6.85 (d, 1H, salicyl phenyl); 6.83 (d, 1H, salicyl phenyl); 6.72 (dd, 2H, 10.9 Hz,*H*(Ph)-C=CH$_2$); 6.62 (d, 2H, salicyl phenyl); 6.57 (d, 2H, salicyl phenyl); 6.40 (dd, 1H, imidazole); 6.57 (dd, 1H, imidazole); 6.13 (dd, 1H, salicyl phenyl); 6.10 (dd, 2H, salicyl phenyl); 5.76 (dd, 2H, trans H(Ph)C=C*H*$_2$); 5.76 (m, 1H, −C*H*$_2$−); 5.67 (dd, 1H, 10.9 Hz, −C*H*$_2$−); 5.25 (dd, 2H, 0.6 Hz, cis H(Ph)C=C*H*$_2$); 5.04 (m, 4H, PhO−C*H*$_2$Ph); 3.56 (t, 1H, −C*H*$_2$−); 3.41 (m, 5H, −C*H*$_2$− and imidazole −NC*H*$_3$); 2.74 (td, 1H, −C*H*$_2$−); 2.40 (m, 1H, −C*H*$_2$−); 2.13 (broad singlet, 1H, −C*H*$_2$−); 1.96 (s, 3H, −CH$_2$CH$_2$CH$_2$N−C*H*$_3$); 1.84 (d, 1H, −C*H*$_2$−); 1.75 (d, 1H, −C*H*$_2$−). IR (KBr): 3155 (vw), 3082 (vw), 3005 (vw), 2933 (vw), 1755 (vw), 1625 (s), 1604 (s), 1535 (m), 1514 (w, sh), 1489 (w), 1474 (w), 1461 (w), 1436 (m, sh), 1429 (m), 1385 (m), 1363 (w), 1302 (m), 1226 (m), 1192 (s), 1121 (m), 1043 (w), 1016 (w), 1001 (m), 988 (w, sh), 961 (w, 923 (w), 910 (w), 846 (s, sh), 832 (s), 795 (w, sh), 737 (w), 659 (w), 623 (w), 557 (m), 459 (w) cm^{-1}. UV−vis (CH_2Cl_2, λ_{max}/nm (ϵ, M^{-1} cm^{-1})): 279 (70 000), 373 (9700), 450 (sh, 850), 651 (350).

(8) Perrin, D. D.; Armarego, W. L. F. *Purification of Laboratory Chemicals*, 3rd ed.; Pergamon Press: New York, 1988.

(9) Daly, J.; Horner, L.; Witkop, B. *J. Am. Chem. Soc.* **1961**, *83*, 4787−4792.

(10) Krebs, J. F. Ph.D. Thesis, 1998, Kansas State University.

Table 1. Crystallographic Data for [Co^{III}1(dmap)$_2$][PF$_6$] and[Co^{III}2(1-MeIm)][PF$_6$]

complex	[Co^{III}**1**(dmap)$_2$][PF$_6$]	[Co^{III}**2**(1-MeIm)][PF$_6$]
molecular formula	$C_{48}H_{50}CoF_6N_6O_4P$	$C_{43}H_{47}CoF_6N_5O_4P$
fw	978.84	944.22
T (K)	298(2)	100(2)
space group	$P21/c$	$P21/c$
a (Å)	19.881(7)	12.5173(13)
b (Å)	13.689(7)	15.0638(16)
c (Å)	18.404(7)	23.074(2)
α (deg)	90	90
β (deg)	112.87(3)	96.75
γ (deg)	90	90
Z	4	4
V (Å^3)	4615(4)	4320.6(7)
δ_{calc} (g/cm^3)	1.409	1.452
R[a]	0.0740	0.0773
R_w[b]	0.1203	0.1451
GOF[c]	1.058	0.928

[a] $R = [\Sigma|\Delta F|/\Sigma|F_o|]$. [b] $R_w = [\Sigma\omega(\Delta F)^2/\Sigma\omega F_o^2]$. [c] Goodness of fit on F^2.

P-2[Co^{III}(1-MeIm)][PF$_6$]. The complex [Co^{III}**2**(1-MeIm)][PF$_6$] (0.617 g, 0.684 mmol) was dissolved in DMF (total DMF is 6.870 g, 94 mmol, 7.28 mL) and the remaining reagents, ethylene glycol dimethacrylate (EGDMA) (2.55 g, 12.9 mmol) and 2,2′-azobisisobutyronitrile (0.0225 g, 137 mmol), were added to the reaction tube, under argon atmosphere. The tube was then sealed and the reaction mixture placed in an oil bath at ∼60 °C for 24 h. The resulting polymer was placed in a Soxhlet apparatus and washed with methanol for 24 h. The resulting polymer was then dried under vacuum. Yield of the dark green polymer was 2.802 g. [Co] = 198 μmol of Co/g of polymer. Nitrogen analysis: 1.51% found; 1.39% calculated; 1.60% calculated and corrected.

P-2(sal)$_2$. The dark green P-**2**[Co^{III}(1-MeIm)][PF$_6$] polymer (0.487 g) was treated with Na_2EDTA. The solid was then filtered and washed five times with deionized water, three times with methanol, and three times with diethyl ether. The polymer was then dried under vacuum. The isolated P-**2**(sal)$_2$ polymer is light olive in color. Yield of the polymer was 0.424 g. [Co] = 28 μmol of Co/g of polymer. Nitrogen analysis: 0.44% found; 0.20% calculated; 0.41% calculated and corrected.

P-2. The P-**2**(sal)$_2$ polymer (0.319 g) was treated with 1.5 equiv (0.0174 g, 120 μmol) of 3,3′-diamino-*N*-methyldipropylamine using the procedure described for the preparation of P-**1**.[7e] Yield of the yellow/light green polymer was 0.290 g. Nitrogen analysis: 1.22% found; 0.91 calculated; 1.12% calculated and corrected.

P-2[Co^{II}]. The yellow/light green P-**2** (0.117 g) was treated with a methanolic solution of Co(OAc)$_2$ and stirred for 6 h. The polymer was then continuously extracted with methanol in the Soxhlet apparatus for 24 h. The resulting dried polymer was dark beige in color. Yield of the polymer was 0.125 g. [Co] = 142 μmol of Co/g of polymer.

Sample Preparation. UV−vis spectra of the monomeric compounds were obtained in solution with use of a 1.00 cm Suprasil quartz cell. Aluminum samples holders for X-ray absorption measurements were approximately 1 in. square by 1 mm thick and contained a 2 × 20 mm slit. Polymer samples were packed dry between two layers of translucent electrical tape (3M, #1205, Minneapolis, MN). Crystalline inorganic compounds were finely ground using a mortar and pestle and diluted with five times the mass of boron nitride (Johnson Matthey) prior to packing into sample holders.

Physical Methods. All proton nuclear magnetic resonance (^{1}H NMR) spectra were collected on a 400 MHz Bruker spectrometer. Infrared spectra were collected on a Mattson Genesis Series FT-IR spectrometer.

Crystallographic data were collected on single crystals of [Co^{III}**1**(dmap)$_2$][PF$_6$] and [Co^{III}**2**(1-MeIm)][PF$_6$]. The red-brown crystal of [Co^{III}**1**(dmap)$_2$][PF$_6$] was mounted on a Siemans P3 diffractometer. Crystal data and details of the diffraction experiment are listed in Table 1. The cell dimensions were obtained by least-squares refinement of the setting angles for 25 reflections. The structure was solved by using Patterson and Fourier methods. Neutral atom scattering factors (including anomalous scattering) were used. All non-H atoms were refined with anisotropic thermal parameters. Hydrogen atoms were included in calculated positions (C−H = 0.950 Å, B_H = 3.0). Weighted ($w = [\sigma^2(R) + gF^2]^{-1}$) least squares refinement on F was carried out by alternately refining the cation or the anion until the largest shift/esd ratio was equal to 0.02. The final fractional atomic coordinates with thermal parameters and the complete listing of all bond angles and bond distances for [Co^{III}**1**(dmap)$_2$][PF$_6$] can be found in the Supporting Information.

A brown plate-shaped crystal of [Co^{III}**2**(1-MeIm)][PF$_6$], with dimensions of 0.41 × 0.18 × 0.01 mm, was selected for structural analysis. Crystal data and details of the diffraction experiment and subsequent calculations are listed in Table 1. Intensity data for this compound were collected using a Bruker SMART APEX ccd area detector mounted on a Bruker D8 goniometer using graphite-monochromated Mo Kα radiation (λ = 0.71073 Å). The intensity data were measured as a series of ω oscillation frames each of 0.25° for 30 s/frame. The detector was operated in 512 × 512 mode and was positioned 5.04 cm from the sample. Coverage of unique data was 100.0% complete to 26.00° in θ. Cell parameters were determined from a least-squares fit of 1233 peaks in the range 2.22° < θ < 19.32°. From 62 peaks that were measured both at the beginning and end of data collection, the crystal showed a decay of −0.11%. The data were corrected for absorption by the semiempirical method from equivalent reflections giving minimum and maximum transmission factors of 0.7997 and 0.9943. Lorentz and polarization corrections were applied. The data were merged to form a set of 8491 independent data with R(int) = 0.1738. The structure was solved by direct methods and refined by full-matrix least-squares methods on F^2.

Hydrogen atom positions were initially determined by geometry and refined by a riding model. Non-hydrogen atoms were refined with anisotropic displacement parameters. The [Co^{III}**2**(1-MeIm)]$^+$ had one region of disorder that was modeled using two orientations. The occupancies for atoms N1, C2, C3, C24, C25, and C46 refined to 0.681(4) and 0.319(4) for the unprimed and primed atoms. The [PF$_6$]$^-$ was disordered and modeled in two orientations with occupancies of 0.532(4) and 0.468(4) for the unprimed and primed atoms. The solvent region, which occurred on a crystallographic center of symmetry, was disordered.

A total of 729 parameters were refined against 821 restraints and 8491 data to give $wR(F^2) = 0.1451$ and $S = 0.928$ for weights of $w = 1/[\sigma^2(F^2) + (0.0450P)^2]$, where $P = [F_o^2 + 2F_c^2]/3$. The final $R(F)$ was 0.0773 for the 3838 observed, [$F > 4\sigma(F)$], data. The largest shift/su was 0.008 in the final refinement cycle. The final difference map had maxima and minima of 0.672 and −0.527 e/Å^3, respectively. The final fractional atomic coordinates with thermal parameters and the complete listing of bond angles and bond distances for [Co^{III}**2**(1-MeIm)][PF$_6$] can be found in the Supporting Information.

X-ray absorption spectra (XAS) of the polymer samples were collected at the National Synchrotron Light Source at Brookhaven National Laboratory (beam line × 9B), using a Si220 monochromator and low-angle nickel mirror for harmonic rejection. The fluorescence spectra were obtained with a 13-element Ge solid-state detectors (Canberra); a deadtime correction of 3 μs was applied to the data, but the effects of this were minimal, since the total count rate was under 30 000 s^{-1} for each detector. An iron filter (nine absorbance thicknesses) was used to remove most of the scattering signal from the desired Kα fluorescence. Calibration spectra were obtained concurrently as described by Wirt,[11] and the beam energy was calibrated by assigning the first inflection on the absorption edge of a cobalt foil to an energy of 7709.5 eV.[12] On the basis

(11) Wirt, M. D.; Kumar, M.; Ragsdale, S. W.; Chance, M. R. *J. Am. Chem. Soc.* **1993**, *115*, 2146−2150.

of the elemental composition of the polymer samples (~1.4% cobalt by mass), it was calculated that the Co K-edge absorption accounts for approximately 45% of the total absorption at energies just above the edge. This high percentage of absorption is due to the element of interest and necessitated fluorescence correction procedures employing transmission XAS data. Details of these corrections are given in the Supporting Information.

X-ray absorption spectra of $[Co^{III}\mathbf{1}(dmap)_2][PF_6]$ and $[Co^{III}\mathbf{2}$-(1-MeImz)$][PF_6]$ were also obtained at beam line × 9B, while those of the acac, en, and NH_3 cobalt complexes were obtained at the Cornell High Energy Synchrotron Source. Transmission spectra were obtained using a Si 111 monochromator and gas ionization chambers.

Simulation of XAS. Transmission spectra of monomers and fluorescence data of polymer samples were analyzed via algorithms similar to those reported previously[13,14] and now implemented within a macro package for Igor Pro (Wavemetrics, Lake Oswego, OR) graphing/analysis software. XAS were divided by μ_0, the calculated[15] monatomic cobalt K-shell absorption above the K-edge. The EXAFS scattering functions for Co−N/O, and second sphere Co−C absorber−scatterer pairs were calculated by FEFF version 7.02[16] using the crystallographic coordinates of $[Co^{III}\mathbf{3}(1\text{-MeIm})]^+$ (**3**, *N*,*N*′-(3,3′-dipropylamine)bis(salicylideneaminate))[17] and are given in the Supporting Information (Table S2). The similar Co−O and Co−N scattering functions were averaged for use in fitting mixed N/O shells. The amplitude factor, S_0^2, was fixed at 0.85 for the Co−N/O shell and 0.50 for the Co−C shells, on the basis of fits to EXAFS data of $Co(acac)_3$, $[Co(en)_3]Cl_3 \cdot 3H_2O$, and $[Co(NH_3)_6]Cl_3$ (Pfaltz and Bauer); see Table S1 of the Supporting Information. The value of $S_0^2 = 0.85$ is typical for EXAFS of coordination compounds simulated by FEFF.[18] The initial simulation of XAS/μ_0 refined parameters for baseline, edge shape, and two shells of EXAFS scatterers. These refinements are called "XAS ($k^2\chi$)" fits because the weighting scheme for the XAS above the edge is equivalent to that of a uniformly weighted fit of $k^2\chi$ between $k = 2.2$ and 14.3 Å^{-1}.[14] The baseline and edge parameters of the initial fits were used to extract experimental EXAFS spectra (χ). The experimental $k^3\chi$ ($k = [2\, m_e\hbar^{-2}\,(E - 7723\text{ eV})]^{0.5}$) was Fourier filtered and the EXAFS parameters were rerefined using weighted fits with uncertainties estimated according to procedures recommended by the International Workshops on Standards and Criteria in XAFS.[13,19] These are the "FF $k^3\chi$" fits.

Results and Discussion

X-ray Diffraction Studies: $[Co^{III}\mathbf{1}(dmap)_2]^+$ and $[Co^{III}\mathbf{2}(1\text{-MeIm})]^+$. The crystal structures of $[Co^{III}\mathbf{1}$-$(dmap)_2]^+$ and $[Co^{III}\mathbf{2}(1\text{-MeIm})]^+$ were determined as their $[PF_6]^-$ salts, and the resulting thermal ellipsoid diagrams are displayed in Figure 1. Crystallographic data and selected bond distances are presented in Tables 1 and 2. The salen moiety of **1** in $[Co^{III}\mathbf{1}(dmap)_2]^+$ adopts the expected square planar geometry about the cobalt center, with the dmap ligands occupying the axial positions to complete the primary coordination sphere of the Co^{III} ion. The average $Co-N_{imine}$ bond distance is 1.882(5) Å, whereas the $Co-N_{dmap}$ bond lengths are approximately 0.10 Å longer (1.979 Å). The average Co−O distance in $[Co^{III}\mathbf{1}(dmap)_2]^+$ is 1.889(4) Å. These metrical parameters are similar to those found for other six-coordinate Co^{III} complexes with *trans*-pyridine and tetradentate salen-like ligands. Many examples can be found in the Cambridge Structural Database.[20] For example, [*trans*-Co(salen)$(py)_2][B(C_6H_5)_4]$[21] has individual Co−X bond lengths within 0.013 Å of the corresponding bond lengths in $[Co^{III}\mathbf{1}(dmap)_2][PF_6]$, and the difference between the average of all six bond lengths in the two structures is less than 0.001 Å.

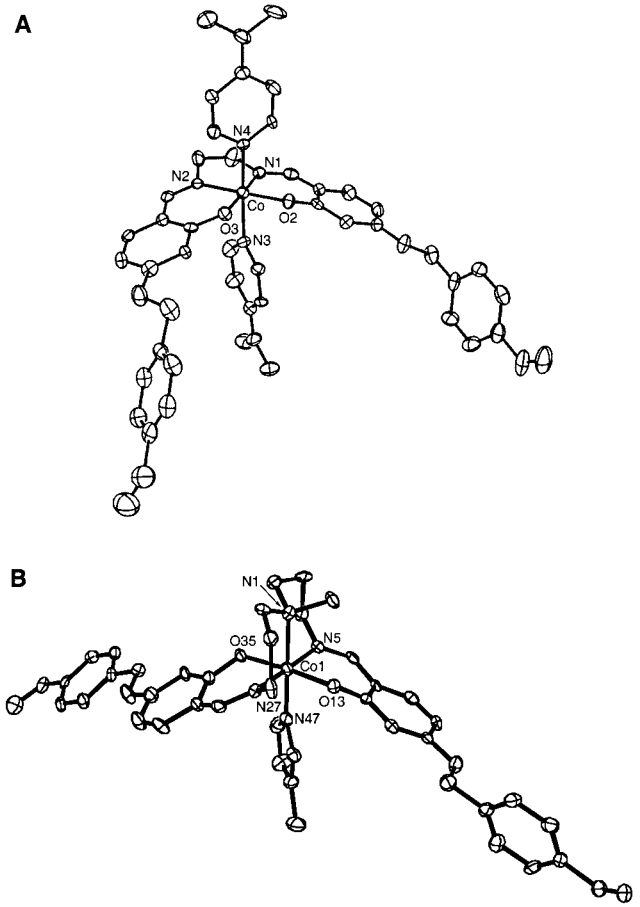

Figure 1. Thermal ellipsoid diagrams of $[Co^{III}\mathbf{1}(dmap)_2]^+$ (**A**) and $[Co^{III}\mathbf{2}(1\text{-MeIm})]^+$ (**B**). The ellipsoids are drawn at the 50% probability level, and hydrogens have been removed for clarity.

Table 2. Selected Bond Distances and Angles for $[Co^{III}1(dmap)_2]^+$ and $[Co^{III}2(1\text{-MeIm})]^+$

$[Co^{III}\mathbf{1}(dmap)_2]^+$	bond lengths (Å)	$[Co^{III}\mathbf{2}(1\text{-MeIm})]^+$	bond lengths (Å)
Co−N1	1.874(7)	Co−O13	1.888(3)
Co−N2	1.891(7)	Co−O35	1.895(3)
Co−N4	1.961(7)	Co−N47	1.932(4)
Co−O3	1.885(6)	Co−N5	1.936(4)
Co−O2	1.893(5)	Co−N27	1.931(4)
Co−N3	1.997(8)	Co−N1	2.031(5)

(12) Bearden, J. A. *Rev. Mod. Phys.* **1967**, *39*, 78−124.
(13) Scarrow, R. C.; Trimitsis, M. G.; Buck, C. P.; Grove, G. N.; Cowling, R. A.; Nelson, M. J. *Biochemistry* **1994**, *33*, 15023−15035.
(14) Scarrow, R. C.; Strickler, B. S.; Ellison, J. J.; Shoner, S. C.; Kovacs, J. A.; Cummings, J. G.; Nelson, M. J. *J. Am. Chem. Soc.* **1998**, *120*, 9237−9245.
(15) McMaster, W. H.; Kerr Del Grande, N.; Mallett, J. H.; Hubbell, J. H. *Compilation of X-ray Cross Sections;* National Technical Information Service, U. S. Chamber of Commerce: Springfield, VA, 1969; *Vol. UCRL-50174 s. II, Rev. 1*.
(16) Ankudinov, A. L.; Rehr, J. J. *Phys. Rev.* **1997**, *B56*, R1712−R1715.
(17) Kistenmacher, T. J.; Marzilli, L. G.; Marzilli, P. A. *Inorg. Chem.* **1974**, *13*, 2089−2093.
(18) O'Day, P. A.; Rehr, J. J.; Zabinsky, S. I.; Brown, G. E., Jr. *J. Am. Chem. Soc.* **1994**, *116*, 2938−2949.
(19) Bunker, G.; Hasnain, S.; Sayers, D. In *X-ray Absorption Fine Structure*, Hasnain, S. S., Ed.; Ellis Horwood: New York; 1991; pp 751−770.
(20) Allen, F. H.; Davies, J. E.; Galloy, J. J.; Johnson, O.; Kennard, O.; Macrae, C. F.; Mitchell, E. M.; Mitchell, G. F.; Smith, J. M.; Watson, D. G. *J. Chem. Inf. Comput. Sci.* **1991**, *31*, 187−204.
(21) Shi, X.; You, X.; Li, C.; Song, B.; Li, T. *Acta Crystallogr.* **1995**, *C51*, 206−207.

Scheme 1[a]

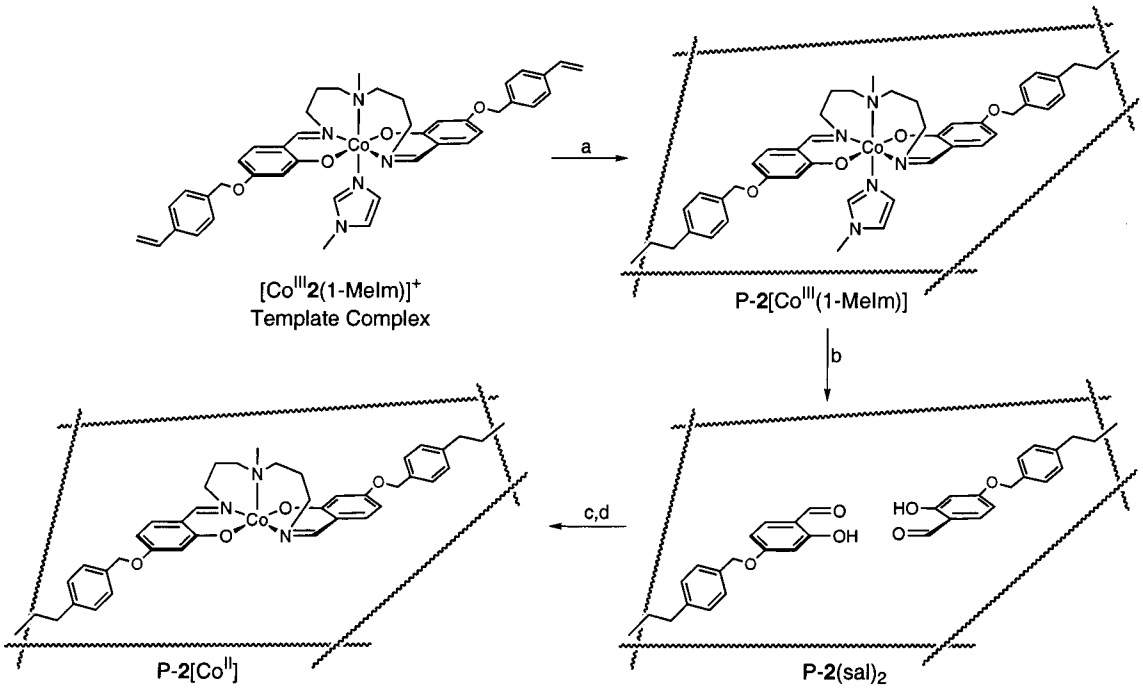

[a] Conditions: a, EGDMA, AIBN, DMF, N_2, 60 °C; b, EDTA, H_2O, Δ; c, $C_7H_{19}N_3$, MeOH; d, $Co(OAc)_2$, MeOH, N_2

The complex $[Co^{III}\mathbf{2}(1\text{-MeIm})]^+$ is also six-coordinate (Figure 1B). The disposition of $\mathbf{2}^{2-}$ around the Co^{III} ion in $[Co^{III}\mathbf{2}(1\text{-MeIm})]^+$ with trans oxygen atoms and trans imine nitrogen atoms has been observed by Kistenmacher[17] for $[Co^{III}\mathbf{3}(1\text{-MeIm})]^+$ and Cini[22] for $[Co^{III}\mathbf{3}'(O_2)]^+$ (**3′**, *N*,*N*′-(3,3′-dipropylmethylamine)bis(salicylideneaminate). These previously reported complexes have pentadentate ligands such as that found in $[Co^{III}\mathbf{2}(1\text{-MeIm})]^+$, the major difference being that they do not contain the polymerizable 4-vinylbenzyloxy groups used in $\mathbf{2}^{2-}$. The Co^{III} bond lengths are similar in these three complexes. For example, average $Co-N_{imine}$ and Co−O distances of 1.923(5) and 1.890(4) Å are found for $[Co^{III}\mathbf{2}(1\text{-MeIm})]^+$, while in $[Co^{III}\mathbf{3}(1\text{-MeIm})]^+$ these bond lengths are 1.922(5) and 1.890(5) Å.

Note that the Co−ligand bond distances involving the chelating ligands $\mathbf{1}^{2-}$ and $\mathbf{2}^{2-}$ in $[Co^{III}\mathbf{1}(dmap)_2]^+$ and $[Co^{III}\mathbf{2}(1\text{-MeIm})]^+$ are nearly identical. The major difference in these metrical parameters is the long $Co-N_{amine}$ distance (2.031(5) Å) found in $[Co^{III}\mathbf{2}(1\text{-MeIm})_2]^+$, which is absent in $[Co^{III}\mathbf{1}(dmap)_2]^+$. In $[Co^{III}\mathbf{2}(1\text{-MeIm})]^+$ the propylene groups and the coordinated tertiary amine are disordered 68:32 over two crystallographically distinct positions. For both $[Co^{III}\mathbf{1}(dmap)_2]^+$ and $[Co^{III}\mathbf{2}(1\text{-MeIm})]^+$, the 4-vinylbenzyloxy groups extend outward from the metal center and cause no apparent distortion of the primary coordination sphere about the Co^{III}.

X-ray Absorption Studies. X-ray absorption spectroscopy has been used to investigate the structure of the cobalt complexes immobilized in polymers P-**1**$[Co^{III}(dmap)_2]$, P-**2**$[Co^{III}(1\text{-MeIm})]$, P-**1**$[Co^{II}]$, and P-**2**$[Co^{II}]$. The immobilized sites were made by template copolymerization methods using the monomeric precursors $[Co^{III}\mathbf{1}(dmap)_2]^+$ and $[Co^{III}\mathbf{2}(1\text{-MeIm})]^+$ and the cross-linking agent EGDMA. Both of these monomeric complexes are substitutionally inert in solution under the polymerization conditions.[7c,e] It was therefore anticipated that the monomers and complexes immobilized in P-**1**$[Co^{III}(dmap)_2]$ and P-**2**$[Co^{III}(1\text{-MeIm})]$ should retain their structures. To examine retention of template structure after polymerization, XAS results on the these polymers were compared with those obtained for the monomers $[Co^{III}\mathbf{1}(dmap)_2]^+$ and $[Co^{III}\mathbf{2}(1\text{-MeIm})]^+$, whose structures were independently determined by X-ray diffraction methods (vide supra). Evaluation of the EXAFS fitting methods used were made by analyzing the structural properties of the known complexes $Co(acac)_3$, $[Co(en)_3]Cl_3 \cdot 3H_2O$, and $[Co(NH_3)_6]Cl_3$. These results are included in the following discussion for completeness. Last, the structural properties of the Co^{II}-containing polymers P-**1**$[Co^{II}]$ and P-**2**$[Co^{II}]$ were examined. These Co^{II}-containing polymers are made, via three-step syntheses, from either P-**1**$[Co^{III}(dmap)_2]$ or P-**2**$[Co^{III}(1\text{-MeIm})]$, their corresponding polymers containing immobilized Co^{III} complexes. The synthetic procedures for the P-**2** polymers are outlined in Scheme 1.

XANES Results for the Co^{III} Systems. The XANES data of $[Co^{III}\mathbf{1}(dmap)_2]^+$ and $[Co^{III}\mathbf{2}(1\text{-MeIm})]^+$ display a preedge peak at 7711 eV (Table 3) that is assigned to a 1s→3d transition (Figure 2). The relatively small size of this peak (2−3% of the edge height with an area of 0.05 eV × edge height) is similar to that of six-coordinate synthetic complexes. The small size of this peak is characteristic of transition metals in centrosymmetric (octahedral or square planar) coordination sites. The second preedge feature is a shoulder at ∼7719 eV,

(22) Cini, R.; Orioli, P. *J. Chem. Soc., Chem. Commun.* **1981**, 196−198.

Table 3. Refined Edge and Pre-edge Parameters from XAS ($k^2\chi$) Fits[a]

sample	E_{edge} (eV)[b]	$E_{1s\rightarrow 3d}$ (eV)[c]	$area_{1s\rightarrow 3d}$ (eV)[c]	$E_{1s\rightarrow 4p}$ (eV)[c]	$area_{1s\rightarrow 4p}$ (eV)[c]
$Co(acac)_3$	7722.91(7)[d]	7710.48(6)	0.058(3)	7715.1(1)	0.033(3)
$[Co(en)_3]^{3+}$	7721.52(2)	7710.59(4)	0.059(3)	7717.32(4)	0.095(8)
$[Co(NH_3)_6]^{3+}$	7722.44(3)	7710.59(4)	0.058(2)	7717.84(3)	0.122(7)
$[Co^{III}\mathbf{1}(dmap)_2]^+$	7724.4(4)	7710.68(4)	0.052(2)	7719.73(5)	0.13(1)
$[Co^{III}\mathbf{2}(1\text{-MeIm})]^+$	7722.9(1)	7710.32(5)	0.046(2)	7719.44(8)	0.07(1)
P-**1**$[Co(dmap)_2]$	7724.3(2)	7710.86(4)	0.061(3)	7719.79(7)	0.10(1)
P-**2**[Co(1-MeIm)]	7722.95(9)	7710.67(3)	0.050(2)	7719.78(8)	0.036(6)
P-**1**$[Co^{II}]$	7719.49(2)	7709.9(1)	0.06(1)	7715.30(2)	0.32(3)
P-**2**$[Co^{II}]$	7718.96(1)	7709.87(3)	0.112(3)	7716.9(1)	0.027(5)

[a] XAS are fit to $(XAS/\mu_0)_{sim}$ = baseline + $\Delta\mu_{edge}(edge_{sim} + \sum peak_i + \chi_{sim})$, where baseline is a cubic function with smooth spline points at 7873 and 8173 eV. Additional details and refined EXAFS parameters are presented in the Supporting Information (Table S14). [b] Midpoint of edge ($edge_{sim}$ is the integral of a 75% Gaussian/25% Lorenzian peak[13]). [c] The two preedge peaks are modeled as Gaussian peaks with refined widths at half-height (constrained to be equal for the two peaks) of 2−3 eV. [d] The esd of the last reported digit (as determined by the least-squares fitting routine) is shown in parentheses.

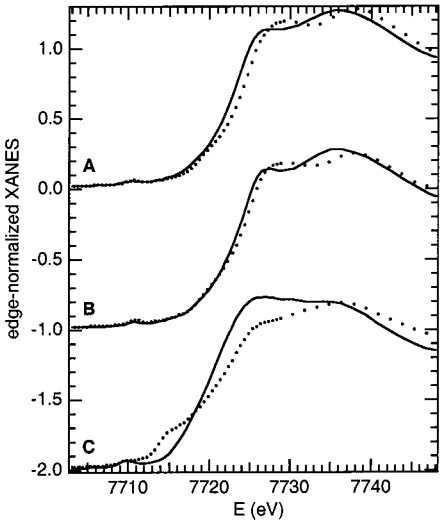

Figure 2. Edge spectra = $[(XAS/\mu_0)$ - baseline$]/\Delta\mu_{edge}$ using baseline and $\Delta\mu_{edge}$ from XAS ($k^2\chi$) fits. For each comparison, XAS of a complex derived from ligand **1** (····) is compared with XAS of a complex derived from ligand **2** (—). (A) Monomer ternary complexes $[Co^{III}\mathbf{1}(dmap)_2]^+$ and $[Co^{III}\mathbf{2}(1\text{-MeIm})]^+$; offset = 0. (B) Polymer ternary complexes P-**1**$[Co^{III}(dmap)_2]$ and P-**2**$[Co^{III}$(1-MeIm)]; offset = −1. (C) Polymer Co^{II} complexes P-**1**$[Co^{II}]$ and P-**2**$[Co^{II}]$; offset = −2.

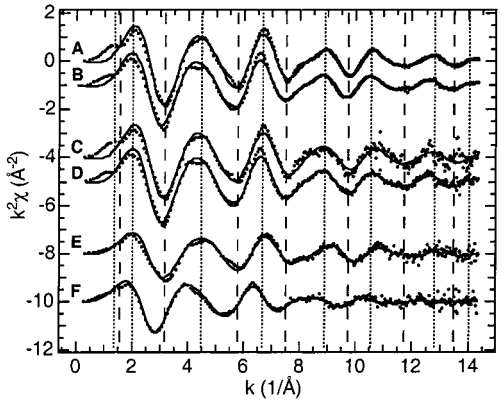

Figure 3. Comparison of EXAFS spectra (····) and simulations (—) from the XAS ($k^2\chi$) refinements. (A) $[Co^{III}\mathbf{1}(dmap)_2]^+$; offset = 0. (B) $[Co^{III}\mathbf{2}(1\text{-MeIm})]^+$; offset = −1. (C) P-**1**$[Co^{III}(dmap)_2]$; offset = −4. (D) P-**2**$[Co^{III}$(1-MeIm)]; offset = −5. (E) P-**1**$[Co^{II}]$; offset = −8. (F) P-**2**$[Co^{II}]$; offset = −10. Vertical lines indicate maxima and minima in the experimental $k^2\chi$ of $[Co\mathbf{1}(dmap)_2]^+$ and are included to aid in comparison of the spectra.

revealed by our edge fitting procedure, assigned to a 1s→4p transition (Table 3).

The XANES data for P-**1**$[Co^{III}(dmap)_2]$ and P-**2**$[Co^{III}$-(1-MeIm)] are virtually indistinguishable from the spectra of their monomeric precursors, $[Co\mathbf{1}(dmap)_2]^+$ and $[Co\mathbf{2}(1\text{-MeIm})]^+$, as shown in Figure 2 and Table 3. The minor differences observed between the two spectra of the monomer complexes are also present in spectra of the corresponding polymer samples. In the XANES region, features near the top of the edge are shifted about 2 eV lower in energy for $[Co^{III}\mathbf{2}(1\text{-MeIm})]^+$ and P-**2**$[Co^{III}$(1-MeIm)] compared to P-**1**$[Co^{III}(dmap)_2]$. One small difference between the monomeric and polymeric samples is that the XANES region for the polymer samples P-**1**$[Co^{III}(dmap)_2]$ and P-**2**$[Co^{III}$(1-MeIm)] have sharper preedge peaks. A Si(220) monochromator was used to obtain spectra of these polymer samples, which provides higher resolution, compared to the spectra collected by the Si(111) monochromator for the monomer samples. The refined areas of the 1s→3d preedge peaks (Table 3) vary by only about 10% between the respective polymers and the monomers. This slight variation is similar to the least-squares uncertainty estimates, indicating that the difference in preedge peak shape can be attributed to the change in monochromators and not structural differences.

EXAFS Results for the CoIII Systems: $[Co\mathbf{1}(dmap)_2]^+$ and $[Co\mathbf{2}(1\text{-MeIm})]^+$. EXAFS data of both $[Co^{III}\mathbf{1}(dmap)_2]^+$ and $[Co^{III}\mathbf{2}(1\text{-MeIm})]^+$ can be fit well with a two shell model using approximately six nitrogen and/or oxygen atoms at ∼1.9 Å and approximately 10 carbon atoms at ∼2.8 Å. The fits to $k^2\chi$ from the XAS ($k^2\chi$) refinements are shown in Figure 3 and refined EXAFS parameters are provided in the Supporting Information. To confirm the results of the refinements on $k^2\chi$, and to estimate parameter uncertainty ranges by the method recommended by the International Workshops on Standards and Criteria in XAS,[19] we also performed weighted fits to Fourier filtered $k^3\chi$. The refined parameters from XAS ($k^2\chi$) (Table S14) and FF $k^3\chi$ (Table 4) fits are virtually identical. The only systematic change due to Fourier filtering is a reduction by about 5% in the refined *n* for the first shell scatterers.

For comparison, Table 4 includes in parentheses the values expected for *n* and *r* for the first (Co−N/O) and second (two Co−C bonds) coordination spheres based on the crystal structures of the monomer precursors. The EXAFS simulations slightly underestimate *n* for the first shell (by about 10%) and estimate *r* to be about 0.02 Å shorter than the average distances found from crystallography. While these discrepancies are minor

Table 4. Refined Parameters and Uncertainty Ranges for Weighted[a] Fits of Fourier Filtered[b] $k^3\chi$ (FF $k^3\chi$ Fits)[c]

	N/O shell[d]		C shell[d]				
sample	n	r (Å)	n	r (Å)	σ (Å)[e]	ΔE_0 (eV)[f]	$\epsilon_\nu{}^{2g}$
[Co^{III}**1**(dmap)$_2$]$^+$	5.6 ± 0.5[h] (6)	1.897 ± 0.007 (1.917)	10 ± 2 (10)	2.84 ± 0.02 (2.87)	0.055 ± 0.009	0.6 ± 1.1	2.8
[Co^{III}2(1-MeIm)$^+$	5.5 ± 0.6 (6)	1.914 ± 0.008 (1.935)	11 ± 2 (11)	2.87 ± 0.02 (2.902)	0.061 ± 0.009	0.0 ± 1.2	1.3
P-**1**[Co(dmap)$_2$]	5.3 ± 0.5	1.898 ± 0.007	9 ± 2	2.82 ± 0.02	0.053 ± 0.009	0.3 ± 1.2	8.1
P-**2**[Co(1-MeIm)]	5.5 ± 0.6	1.913 ± 0.007	10 ± 2	2.86 ± 0.02	0.058 ± 0.009	−0.1 ± 1.2	1.8
P-**1**[Co^{II}]	3.4 ± 0.5	1.859 ± 0.011	6 ± 2	2.80 ± 0.03	0.054 ± 0.015	−2.0 ± 2.0	0.5
P-**2**[Co^{II}]	4.8 ± 0.9	1.962 ± 0.016	9 ± 3	2.91 ± 0.04	0.090 ± 0.015	−2.3 ± 2.3	0.5

[a] Esd_{FF} is interpolated from the following (k·Å, esd_{FF}·Å^3): (2.2, 0.14), (4, 0.19), (8, 0.26), (10, 0.42), (13, 0.88), (14.3, 0.56).[13] [b] Fourier filtered $k^3\chi$ and $k^3\chi_{sim}$ are denoted FF and FF_{sim}, respectively. Fourier transform: $k = 1.0-14.3$ Å^{-1} using 5% windowing.[13] Back-transform: $r' = 0.90-2.45$ Å. [c] Crystallographic data are in parentheses when available: average bond lengths and two-bond Co−C distances from crystal structures. [d] EXAFS from each shell ($\chi_{sim} = \chi_1 + \chi_2$) is modeled as $\chi_i = S_0{}^2 n_i f_i \exp(-2k_i{}^2\sigma_i{}^2)k_i{}^{-1}r^{-2}\sin(2k_i r_i + \alpha_i)$. $e\sigma_2$ was constrained equal to σ_1. Without this constraint, σ_2 refined to less than σ_1, which is unrealistic. [f] The k_i used in calculating χ_{sim} is $k_i = [2m_e\hbar^{-2}(E - (7723\text{ eV} + \Delta E_0))]^{0.5}$. [g] The minimized residual, $\epsilon_\nu{}^2 = [n_{idp}/(n_{idp} - n_{par})] \times \text{average}\{(FF - FF_{sim})/esd_{FF}\}^2$, where n_{par} = number of refined parameters and n_{idp} = number of independent data points = 2(2.45−0.90 Å)(14.3−2.2 Å^{-1})/π = 11.9.[19] [h] The uncertainty range is that over which the parameter can be fixed (while refining other parameters) without increasing $\epsilon_\nu{}^2$ by more than 1.0 above the minimized value.[19] The allowed positive and negative deviations from the refined value were similar (within 10%); the average of these deviations is reported as the ± quantity.

(and within limits generally considered acceptable for EXAFS analysis), they appear to be systematic—always toward slight underestimation of n and r. These systematic effects are attributed, at least in part, to deficiencies of the Debye−Waller term ($\exp(-2k_i{}^2\sigma_i{}^2)$) in modeling the >0.1 Å range of bond lengths and the neglect of third sphere and multiple scattering EXAFS by the two-shell simulations.[23]

P-1[Co^{III}(dmap)$_2$] and P-2[Co^{III}(1-MeIm)]. The refined EXAFS parameters (Table 4) of the polymer and monomer samples are the same, each having overlapping estimated standard deviation or uncertainty ranges. The marginal exceptions are for the second sphere upon conversion of [Co^{III}**1**(dmap)$_2$]$^+$ to the polymer P-**1**[Co^{III}-(dmap)$_2$]; there is a decrease in r(Co−C) by 0.02 Å and (in the XAS ($k^3\chi$) fits) an increase in σ(Co−C) from 0.045 ± 0.006 to 0.07 ± 0.01 Å. In addition, the Fourier transform of $k^2\chi$ (Figure 4) also suggests minor differences in the second sphere coordination environment between the [Co^{III}**1**(dmap)$_2$]$^+$ monomer and P-**1**[Co^{III}-(dmap)$_2$]$^+$. Such differences may be caused by steric crowding of the dmap and/or salen ligands in the immobilized sites. However, the relatively small changes in the EXAFS data and refined parameters indicate that distortions caused by steric crowding are minor.

Even the higher frequency EXAFS, resulting from longer path length scattering paths, is similar between the monomer and polymer samples; note the similarities in the EXAFS difference spectra shown in Figure 5, in which the two shell simulations are subtracted from the data. Thus, the EXAFS data provide strong evidence that the cobalt coordination environment is changed only slightly during the polymerizations of [Co^{III}**1**-(dmap)$_2$]$^+$ and [Co^{III}**2**(1-MeIm)]$^+$. Figure 5 also shows the difference spectrum from fitting the FEFF multiple scattering simulation using the coordinates of [Co^{III}**1**-(dmap)$_2$]$^+$. This difference spectrum represents the predicted EXAFS spectrum from multiple scattering and third and higher coordination shells. Positions of minima and maxima are similar to the observed residual $k^2\chi$ spectrum obtained by fitting the two shell fits to [Co**1**(dmap)$_2$]$^+$, particularly in the region between k =4−8 Å^{-1}. This suggests that this region of the EXAFS spectrum contains oscillations caused by longer single and multiple scattering pathways characteristic of the salen and/or dmap ligands.

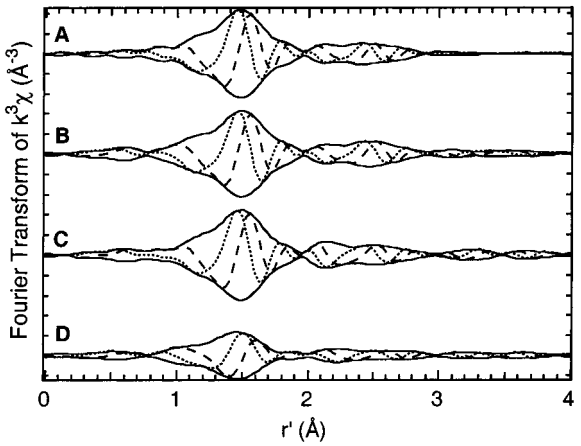

Figure 4. Fourier transforms of $k^3\chi$ from EXAFS of cobalt complexes of [Co^{III}**1**(dmap)$_2$]$^+$ and [P-**1**Co^{III}(dmap)$_2$][PF_6]. Each FT is shown with a real (····) and imaginary (---) component enclosed within a FT magnitude envelope (—). (A) FF $k^3\chi$ fit for EXAFS of [Co^{III}**1**(dmap)$_2$]$^+$. (B) EXAFS data for [Co^{III}**1**-(dmap)$_2$][PF_6]. (C) EXAFS data for [P-**1**Co^{III}(dmap)$_2$][PF_6]. (D) EXAFS data for P-**1**[Co^{II}].

Synthesis of P-1[CoII] and P-2[CoII]. The functions of the Co^{II}-containing polymers P-**1**[Co^{II}] and P-**2**[Co^{II}] are to reversibly bind nitric oxide and dioxygen.[7c−e] Binding of these gaseous molecules in the polymers occurs at the immobilized metal centers and necessitates that Co^{II} ions be present. The synthetic process to convert the original templated Co^{III}-containing polymers, P-**1**[Co^{III}(dmap)$_2$] and P-**2**[Co^{III}(1-MeIm)], to polymers with Co^{II} complexes is outlined in Scheme 1 for the polymer containing ligand **2**. The immobilized metal complexes in P-**1**[Co^{III}(dmap)$_2$] and P-**2**[Co^{III}-(1-MeIm)] are inert and require the addition of [EDTA]$^{2-}$

(23) Support for this statement comes from simulations using FEFF 7.02 and the non-hydrogen atom coordinates of the monomers. Single and multiple scattering paths were included for out-and-back path length <12 Å. When these simulations were treated as data sets and fit by the same protocol as used in Table 4, the refined r and first sphere n were lower than crystallographic values by amounts that were (on average) at least half as large as the deviations of the refined EXAFS parameters (Table 4) from crystallographic values. These simulations also show that the low $S_0{}^2$ found for the second sphere Co−C scattering is due to destructive interference in the EXAFS amplitude caused by third sphere and multiple scattering EXAFS. (See Table S15 in the Supporting Information).

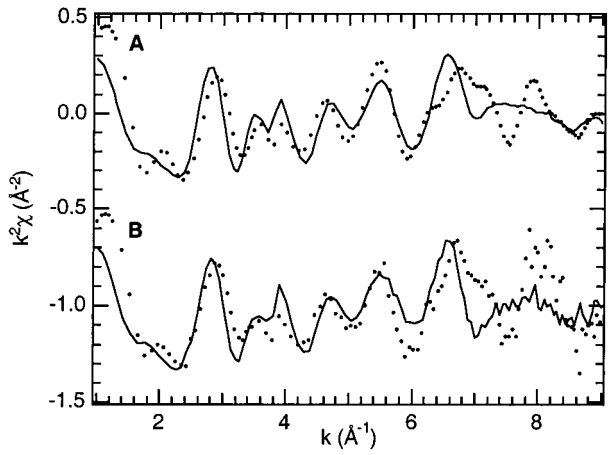

Figure 5. Difference $k^2\chi$ spectra (obs − calc) using parameters from FF $k^3\chi$ fits (Table 4) for six-coordinate monomeric complexes. (A) $[Co^{III}\mathbf{1}(dmap)_2]^+$ (····) and $[Co^{III}\mathbf{2}(1\text{-MeIm})]^+$ (—); offset = 0. (B) Corresponding polymers P-**1**$[Co^{III}(dmap)_2]$ (····) and P-**2**$[Co^{III}(1\text{-MeIm})]$ (—); offset = −1. Beyond $k = 9$ Å^{-1} the differences between the difference spectra are obscured by noise.

under conditions of relatively low pH to remove the Co^{III} ions. These conditions also hydrolyze the immobilized diimine ligands **1** and **2** back to their corresponding salicylaldehyde moieties, which remain covalently attached to the porous organic host (P-**1**$(sal)_2$ and P-**2**$(sal)_2$).[7c,e] The predisposition of the salicylaldehyde groups allows for regeneration of the diiminediphenol ligands within the porous host. This is accomplished by treating methanolic suspensions of P-**1**$(sal)_2$ with ethylenediamine to afford P-**1** and P-**2**$(sal)_2$ with 3,3′-diamino-*N*-methyldipropylamine to yield P-**2**. Both of these "apo" polymers readily rebind Co^{II} ions to form P-**1**$[Co^{II}]$ and P-**2**$[Co^{II}]$. EPR spectroscopy and gas binding studies have suggested that the Co^{II} ions rebind as expected to these rebuilt immobilized sites; that is, four-coordinate Co^{II} complexes are immobilized in P-**1**$[Co^{II}]$, whereas P-**2**$[Co^{II}]$ has five-coordinate complexes. The reported XAS experiments were conducted to further examine the structural properties of these immobilized Co^{II} complexes in P-**1**$[Co^{II}]$ and P-**2**$[Co^{II}]$.

XANES Results for P-1[Co^{II}] and P-2[Co^{II}]. The XANES spectra for P-**1**$[Co^{II}]$ and P-**2**$[Co^{II}]$ are found in Figure 2 and results are listed in Table 3. The K-edge energies in the XANES spectra for the two Co^{II}-containing polymer are similar at 7719.49 (P-**1**$[Co^{II}]$) and 7718.96 eV (P-**2**$[Co^{II}]$). These K-edges are shifted to lower energy by about 3 eV relative to the spectra for the Co^{III} monomers and polymers. This is consistent with the additional electron density of the Co^{II} centers. In addition, a pronounced shoulder at 7715.3 eV is observed in the spectrum of P-**1**$[Co^{II}]$ and is attributed to a 1s→4p transition. The prominence of this feature relative to the 1s→3d transition at 7709.9 eV is indicative of square planar geometries, based on XANES studies of a variety of nickel coordination compounds.[24]

EXAFS Results for P-1[Co^{II}] and P-2[Co^{II}]. The analysis of the EXAFS of these Co^{II} polymer samples shows the expected decrease in coordination number. Data for P-**1**$[Co^{II}]$ also indicate a significant decrease in the number of second sphere Co−C scatterers. The refined bond lengths (and Co−C distances) decrease for four-coordinate P-**1**$[Co^{II}]$ relative to the six-coordinate Co^{III} centers in $[Co^{III}\mathbf{1}(dmap)_2]^+$ and P-**1**$[Co^{III}(dmap)_2]$. The shortening of bond lengths generally observed with a decrease in coordination number from six to four outweighs the bond lengthening expected upon reduction of the cobalt.[25] The refined bond lengths and Co−C distances for five-coordinate P-**2**$[Co^{II}]$ are significantly longer than for the corresponding six-coordinate Co^{III} complexes. The refined average bond lengths in P-**1**$[Co^{II}]$ and P-**2**$[Co^{II}]$ (1.86 and 1.96 Å, respectively) are similar to those in square planar and square pyramidal Co^{II} Schiff base complexes such as *meso*-(*N*,*N*′-cyclohexylenebis(salicylideneiminato)cobalt(II) (average *r*(Co−X) = 1.866 Å)[26] and $[Co^{II}\mathbf{4}(pyridine)]$ (**4**, *N*,*N*′-(2,3-butylene)bis(salicylideneiminate)) (average *r*(Co−X) = 1.937 Å).[27]

The crystal structure of five-coordinate $[Co^{II}4\text{-(pyridine)}]$ has a second molecule of approximate trigonal bipyramidal geometry with an average *r*(Co−X) of 2.042 Å. In addition, trigonal bipyramidal coordination geometries and longer average Co−X bond lengths appear to be favored by the 3,3′-dipropylamine bridge between the two salicylidenimine groups as is found in ligands **2**, **3**, and **3′**. A search of the Cambridge Structural Database[20] found three structures (with different cocrystallized molecules) containing a $[Co^{II}\mathbf{3}']$ molecule, and one of a closely related molecule with *tert*-butyl substituents.[22,28] All of these adopt a trigonal bipyramidal geometry and have average *r*(Co−X) values ranging from 2.024 to 2.046 Å. The refined average *r*(Co−X) for P-**2**$[Co^{II}]$ of 1.96, determined by EXAFS analysis, is near the 1.937 value observed for square pyramidal Co^{II} complexes with Schiff base ligands. It is important to note that ligand **2** in the template complex $[Co^{III}\mathbf{2}(1\text{-MeIm})]^+$, which was used to form the immobilized sites in P-**2**$[Co^{III}(1\text{-MeIm})]$, also adopts a square pyramidal coordination geometry about the Co^{III} ion. Subsequent demetalation, hydrolysis, reformation of **2**, and Co^{II} ion binding do not significantly alter the coordination properties of the immobilized ligands. That is, the porous organic host does not allow ligand **2** to fully distort to form trigonal bipyramidal Co^{II} complexes (with longer bond lengths) as preferred for monomeric analogues.

Summary and Conclusions. This study illustrates that the structures of inert metal templates are retained upon copolymerization with organic cross-linking agents. Materials made by this method contain immobilized metal complexes in porous organic hosts. We have used XAS to probe the structures of immobilized cobalt complexes in porous methacrylate hosts. The structural properties of the immobilized cobalt complexes obtained from XAS measurements match those found for their monomeric precursors.[29] EXAFS data yielded first and second shell parameters for the cobalt complexes in

(24) Colpas, G. J.; Maroney, M. J.; Bagyinka, C.; Kumar, M.; Willis, W. S.; Suib, S. L.; Baidya, N.; Mascharak, P. K. *Inorg. Chem.* **1991**, *30*, 920−928.
(25) Shannon, R. D. *Acta Crystallogr.* **1976**, *A32*, 751−767.
(26) Bresciani, N.; Calligaris, M.; Nardin, G.; Randaccio, L. *J. Chem. Soc., Dalton Trans.* **1974**, 1606−1609.
(27) Bresciani, N.; Calligaris, M.; Nardin, G.; Randaccio, L. *J. Chem. Soc., Dalton Trans.* **1974**, 498−502.
(28) (a) Cini, R.; Orioli, P. *Inorg. Chim. Acta*, **1982**, *63*, 243−248. (b) Boca, R.; Elias, H.; Haase, W.; Huber, M.; Klement, R.; Müller, L.; Paulus, H.; Svoboda, I.; Valko, M. *Inorg. Chim. Acta* **1998**, *278*, 127−135.

P-**1**[Co^{III}(dmap)$_2$] that are statistically identical to those for the template [Co^{III}**1**(dmap)$_2$]$^+$. Similar findings were obtained for P-**2**[Co^{III}(1-MeIm)] and its corresponding template [Co^{III}**2**(1-MeIm)]$^+$. The structural properties of the template complexes obtained from EXAFS data were independently verified using results from X-ray diffraction studies on single crystals of [Co^{III}**1**(dmap)$_2$][PF_6] and [Co^{III}**2**(1-MeIm)][PF_6].

P-**1**[Co^{III}(dmap)$_2$] and P-**2**[Co^{III}(1-MeIm)] are converted to the Co^{II}-containing polymers P-**1**[Co^{II}] and P-**2**[Co^{II}] via a three-step synthesis involving the hydrolysis of imine bonds in the multidentate ligands **1** and **2**. These polymer-bound ligands can be reformed within the cavities by treatment with the appropriate di- or triamine. XANES results for P-**1**[Co^{II}] and P-**2**[Co^{II}] show K-edge energies that are consistent with the coordination expected for Co^{II} ions. EXAFS data of the immobilized metal sites in P-**1**[Co^{II}] indicate that the coordination environments adopted by the Co^{II} ions are similar to those observed for monomeric Co^{II} Schiff base complexes. Additionally, a square pyramidal coordination geometry is maintained around the immobilized Co^{II} ions in P-**2**[Co^{II}], as opposed to converting to a trigonal bipyramidal arrangement, which is observed in related monomeric Co^{II} complexes. This is an important result because it provides evidence that the organic host regulates the site structure in order to retain the coordination environment of the template complex, even after the immobilized sites have undergone extensive chemical modification. These results corroborate our previous studies that utilize EPR spectroscopy to probe structure/function relationships of materials containing immobilized metals complexes made by template copolymerization techniques.[7c−f]

Porous materials with immobilized metal complexes of defined structure have wide applications in catalysis, gas storage, and sensor technology.[30,31] The use of soluble molecular precursors whose properties are maintained during material formation is advantageous when the same properties are desired in the polymer. This study provides structural data that template copolymerization is an effective method for creating immobilized metal sites in porous hosts. Moreover, chemical modification of the sites affords new centers with predictable metal binding properties.

Acknowledgment. Financial support of this work was provided by ONR-DEPSCoR and NIH. Research carried out (in part) at the National Synchrotron Light Source, Brookhaven National Laboratory, which is supported by the U.S. Department of Energy, Division of Materials Sciences and Division of Chemical Sciences. K.T.T. was partially funded through a NSF-REU grant at the University of Kansas. We thank Dr. Doug Powell of the Molecular Structure Laboratory at the University of Kansas for assistance with the X-ray diffraction analysis.

Supporting Information Available: Complete X-ray data, results from EXAFS and XANES refinements on model complexes, and the amplitude, as well as phase, functions calculated using FEFF 7.02 for Co−N/O and Co−C scattering (PDF). This material is available free of charge via the Internet at http/::pubs.acs.org.

CM010502R

(29) Sato, M. Fujii, Y.; Yamamura, T.; Yano, S. *Bull. Chem. Soc. Jpn.* **1994**, *67*, 1954−1956.
(30) Yaghi, O. M.; Li, H.; Davis, C.; Richardson, D.; Groy, T. L. *Acc. Chem. Res.* **1998**, *31*, 474−484 and references therein.
(31) Golden, J. H.; Deng, H.; DiSalvo, F. J.; Fréchet, J. M. J.; Thompson, P. M. *Science* **1995**, *268*, 1463−1466.